

# Anomalous diffusion, clustering, and pinch of impurities in plasma edge turbulence

M. Priego,\* O. E. Garcia, V. Naulin, and J. Juul Rasmussen

*Association EURATOM–Risø National Laboratory, OPL-128 Risø, DK-4000 Roskilde, Denmark*

(Dated: January 7, 2005)

The turbulent transport of impurity particles in plasma edge turbulence is investigated. The impurities are modeled as a passive fluid advected by the electric and polarization drifts, while the ambient plasma turbulence is modeled using the two-dimensional Hasegawa–Wakatani paradigm for resistive drift-wave turbulence. The features of the turbulent transport of impurities are investigated by numerical simulations using a novel code that applies semi-Lagrangian pseudospectral schemes. The diffusive character of the turbulent transport of ideal impurities is demonstrated by relative-diffusion analysis of the evolution of impurity puffs. Additional effects appear for inertial impurities as a consequence of compressibility. First, the density of inertial impurities is found to correlate with the vorticity of the electric drift velocity, that is, impurities cluster in vortices of a precise orientation determined by the charge of the impurity particles. Second, a radial pinch scaling linearly with the mass-charge ratio of the impurities is discovered. Theoretical explanation for these observations is obtained by analysis of the model equations.

## I. INTRODUCTION

One of the persistent problems in the development of a magnetic fusion reactor is the degradation of plasma confinement caused by turbulent transport. In spite of the strong confining magnetic field, high levels of energy and charged-particle transport across magnetic field lines are observed in a variety of experimental configurations, such as tokamaks and stellarators. This transport has received the adjective “anomalous,” as its features cannot be explained by the classical or neoclassical collisional theories. Instead, anomalous transport is generally attributed to small-scale, electrostatic plasma turbulence.<sup>1,2</sup> In particular, the transport in the plasma edge is believed to be largely controlled by drift-wave turbulence, which appears naturally in this region as a result of the strong radial pressure gradient. The drift-wave transport mechanism has been the subject of much theoretical and experimental research over the past several decades, and was recently reviewed by Horton.<sup>2</sup> Nevertheless, much of this transport phenomenon is yet to be fully understood.

Another important problem in the quest for controlled thermonuclear fusion that is linked to turbulence concerns the impurity content of the plasma. The properties of fusion plasmas are strongly influenced by the presence of impurities. For instance, impurities enhance radiative energy losses and dilute the hydrogen fuel within the hot plasma center, at the same time being the main agents in the erosion and deposition processes that affect plasma-facing components.<sup>3</sup> Consequently, the understanding of the transport mechanisms that control the impurity content in the plasma is of crucial importance for the performance and safe operation of future fusion devices.

The transport of impurity particles across the mag-

netic field is related to that of the bulk plasma, since the motion perpendicular to the magnetic field of all charged particles in the plasma is dominated by one same velocity field, the electric drift velocity. In this sense, impurities and bulk plasma are partly subject to a common mechanism of turbulent transport, which relates the problem of confinement to that of controlling the impurity content. However, the distinctive nature of impurity particles, notably their mass and electric charge, as well as their different influence on the plasma allow for disparities between the transport of impurities and that of the bulk plasma. In fact, recent experiments not only reveal disparities in the transport of impurities and bulk plasma,<sup>4</sup> but also in that of different impurity species.<sup>5</sup> In such experimental investigations impurity transport is usually characterized in terms of effective diffusion coefficients and drift velocities, the latter also known as pinch velocities.<sup>1,6</sup> These transport coefficients are typically determined by analysis of the temporal evolution of injected impurity puffs. While the explanation for the diffusive character of turbulent transport goes back to the work of Taylor and Richardson in the 1920s,<sup>7,8</sup> the origin of the anomalous pinch velocities is still a matter of intense research.<sup>6</sup> Moreover, the inward pinch observed in laboratory experiments tends to concentrate the impurities in the center of the plasma column,<sup>1</sup> precisely where they are least wanted, and thus constitutes one of the major unresolved transport problems in fusion plasma physics.

In this contribution we investigate the turbulent transport of impurities in a generic model for plasma edge turbulence. Specifically, the investigations are based on the simple and extensively studied model for resistive drift-wave turbulence proposed by Hasegawa and Wakatani.<sup>9</sup> For the impurities, we use a consistent passive-fluid model that takes into account impurity-particle inertia, that is to say, it contemplates the polarization drift. This enables the model to exhibit different transport features depending on the mass and charge of the impurities, as observed in laboratory experiments. In particular, the polarization drift brings compressibility into the

---

\*Also at Department of Mathematics, Technical University of Denmark and Departamento de Fluidos y Calor, Universidad Pontificia Comillas–ICAI; E-mail address: martin.priego@telefonica.net

model, giving rise to subtle yet qualitatively important effects. The investigations are carried out by numerical simulations of the model equations using a newly developed code that applies semi-Lagrangian pseudospectral schemes. We proceed separately for ideal (i.e., massless) impurities and inertial ones. In the case of ideal impurities, we focus on the phenomenon of turbulent diffusion, which is studied from the relative-diffusion perspective. For inertial impurities, we concentrate on the new effects that arise from compressibility. First, the density of inertial impurities is found to correlate with the vorticity of the electric drift velocity, that is, impurities cluster in vortices of a precise orientation determined by the charge of the impurity particles. This behavior is a direct consequence of compression by the polarization drift and turbulent mixing. Second, we discover a radial pinch that scales linearly with the mass-charge ratio of the impurities. An understanding of this phenomenon is obtained by analysis of the evolution equation for the global impurity flux.

This paper is organized as follows. In Sec. II the model for resistive drift-wave turbulence and the passive-fluid model for the impurities are described. The diffusive effect of turbulence is demonstrated in Sec. III for the case of ideal impurities. The effects that arise from impurity inertia, the clustering and the anomalous radial pinch, are respectively presented in Secs. IV and V. The results are summarized and discussed in Sec. VI. Lastly, the Appendix is devoted to a brief description of the numerical schemes applied in the simulations.

## II. MODEL EQUATIONS

In this section we provide a brief presentation of the resistive drift-wave paradigm used for modeling the turbulence at the plasma edge. We also describe the passive-fluid model for the impurity species, which takes into account impurity-particle inertia.

### A. Resistive drift-wave turbulence

As a basic model for plasma edge turbulence we consider the two-dimensional (2D) Hasegawa–Wakatani (HW) model for resistive drift-wave turbulence:<sup>9</sup>

$$D_t(n - x) = \mathcal{C}(\varphi - n) + \mu_n \nabla_{\perp}^2 n, \quad (1a)$$

$$D_t \omega = \mathcal{C}(\varphi - n) + \mu_{\omega} \nabla_{\perp}^2 \omega, \quad (1b)$$

where

$$\omega \equiv \nabla_{\perp}^2 \varphi, \quad (1c)$$

$$D_t \equiv \partial_t + \hat{\mathbf{z}} \times \nabla_{\perp} \varphi \cdot \nabla_{\perp}. \quad (1d)$$

Here,  $n$  denotes the fluctuating component of the plasma density,  $\varphi$  is the electrostatic potential, and  $\omega$  is the vorticity of the electric drift velocity  $\mathbf{v}_E = \hat{\mathbf{z}} \times \nabla_{\perp} \varphi$ .

The HW model assumes an unperturbed, uniform magnetic field in the  $z$ -direction, that is,  $\mathbf{B} = B_0 \hat{\mathbf{z}}$ . The  $x$ - and  $y$ -directions correspond respectively to the radial and the poloidal directions in a slab at the edge of the confined plasma. The electrons are assumed isothermal with temperature  $T_e$ , whereas the ions are considered cold. The equilibrium plasma density  $n_0$  is assumed to be homogeneous in the poloidal direction and to decrease in the radial direction in such a way that the equilibrium density length scale  $L_n \equiv n_0/|dn_0/dx|$  is constant. Hence, in this thin-layer approximation the second term on the left-hand side of Eq. (1a) actually represents the advection of the inhomogeneous equilibrium plasma density by the electric drift.

The quantities in Eqs. (1) have been made dimensionless using the gyro-Bohm normalization:

$$\frac{x}{\rho_s} \rightarrow x, \quad \frac{y}{\rho_s} \rightarrow y, \quad t \frac{c_s}{L_n} \rightarrow t, \quad \frac{n}{n_0} \frac{L_n}{\rho_s} \rightarrow n, \quad \frac{e\varphi}{T_e} \frac{L_n}{\rho_s} \rightarrow \varphi.$$

Here,  $c_s \equiv (T_e/m_i)^{1/2}$  is the sound speed and  $\rho_s \equiv (m_i T_e)^{1/2}/eB_0$  is the the drift scale, that is, the ion gyro-radius at the sound speed. The parameter  $\mathcal{C}$  coupling Eqs. (1a) and (1b) is known as the adiabaticity parameter, and is defined as

$$\mathcal{C} \equiv \frac{T_e}{e^2 \eta_{\parallel} n_0} \frac{k_{\parallel}^2}{c_s/L_n}.$$

Here,  $\eta_{\parallel}$  is the parallel resistivity and  $k_{\parallel}$  is the single parallel wave number that is considered in the reduction to a 2D model. In the strongly collisional limit  $\mathcal{C} \rightarrow 0$ , Eq. (1b) reduces to the 2D Navier–Stokes vorticity equation. In this so-called hydrodynamic limit the equations become decoupled and the plasma density is passively advected by the electric drift velocity. In the weakly collisional limit  $\mathcal{C} \rightarrow \infty$ , the adiabatic electron response yields Boltzmann-distributed density perturbations,  $n \approx \varphi$ , and the HW model reduces to the well-known Hasegawa–Mima equation.<sup>10</sup>

The diffusive terms in Eqs. (1a) and (1b) correspond respectively to the collisional diffusion of electrons and the ion viscosity. These dissipative processes are essential for the stabilization of resistive drift modes as well as for the feasibility of numerically simulating the HW model. Linear analysis of the HW model reveals the existence of unstable modes for  $0 < \mathcal{C} < \infty$ , with all modes being unstable in the absence of dissipation.<sup>11,12</sup> It is the combination of this linear instability with nonlinear interaction through the advective terms and dissipation at small scales that leads to quasistationary turbulent states within the HW model. In particular, when initialized with a broadband set of small-amplitude, random-phase modes, the system evolves in two stages: first, a linear phase in which the linearly unstable modes grow and the damped ones decay; second, a phase of nonlinear saturation leading to a quasistationary turbulent state whose statistics solely depend on the parameters of the HW model.

Two relevant nonlinear invariants in the HW model are the total energy  $E$  and the generalized enstrophy  $U$ , defined as

$$E \equiv \frac{1}{2} \int (n^2 + |\nabla_{\perp} \varphi|^2) d\mathbf{x},$$

$$U \equiv \frac{1}{2} \int (n - \omega)^2 d\mathbf{x}.$$

The evolution of these quantities within the HW model is governed by

$$\frac{dE}{dt} = \Gamma_n - \Gamma_c - \mathcal{D}^E,$$

$$\frac{dU}{dt} = \Gamma_n - \mathcal{D}^U,$$

where

$$\Gamma_n \equiv - \int n \partial_y \varphi d\mathbf{x},$$

$$\Gamma_c \equiv \mathcal{C} \int (n - \varphi)^2 d\mathbf{x},$$

$$\mathcal{D}^E \equiv \int (\mu_n |\nabla_{\perp} n|^2 + \mu_{\omega} |\nabla_{\perp} \omega|^2) d\mathbf{x},$$

$$\mathcal{D}^U \equiv \int \nabla_{\perp} (n - \omega) \cdot \nabla_{\perp} (\mu_n n - \mu_{\omega} \omega) d\mathbf{x}.$$

Hence,  $\Gamma_n$  is the only source in the system, and corresponds to energy extracted from the equilibrium density gradient. Conversely,  $\Gamma_c$  is a sink corresponding to resistive dissipation through the parallel current, while  $\mathcal{D}^E$  and  $\mathcal{D}^U$  are sinks arising from collisionality and viscosity. Being the sole source of energy and generalized enstrophy source within the HW model,  $\Gamma_n$  is in practice positive definite.<sup>11</sup> This fact is used in Sec. V to identify a source for radial drift of impurities.

### B. Impurity passive-fluid model

Impurities are here regarded as a passive species, that is, they are advected by the turbulence but do not have any influence on it. This is a reasonable approximation for the situation in which the density of impurity particles is much lower than that of the bulk plasma. The modeling of the dynamics of impurities is consistent with that of the turbulence, in that it also follows from the drift-ordered fluid approach and the assumption of unperturbed, uniform magnetic field.

The impurities are characterized by a density  $\theta$  and a flow velocity  $\mathbf{v}_{\theta}$ . Just as in the case of the ions in the bulk plasma, the impurities are assumed cold, with their motion parallel to the magnetic field likewise being neglected. Therefore, the motion of the impurity fluid comprises only the electric drift  $\mathbf{v}_E$  and the polarization drift  $\mathbf{v}_p$ . Under the same normalization applied to the

turbulence model, the flow velocity of the impurities is hence given by

$$\mathbf{v}_{\theta} = \mathbf{v}_E + \mathbf{v}_p = \hat{\mathbf{z}} \times \nabla_{\perp} \varphi - \zeta \mathbf{D}_t \nabla_{\perp} \varphi,$$

where

$$\zeta \equiv \frac{m_{\theta}}{q_{\theta}} \frac{e}{m_i} \frac{\rho_s}{L_n}.$$

Here,  $m_{\theta}$  and  $q_{\theta}$  are respectively the mass and the electric charge of the impurity particles. The impurity model resulting from the continuity equation is thus given by

$$\mathbf{D}_t \theta - \nabla_{\perp} \cdot (\theta \zeta \mathbf{D}_t \nabla_{\perp} \varphi) = \mu_{\theta} \nabla_{\perp}^2 \theta, \quad (2)$$

where the term on the right-hand side arises from collisional diffusion.

The polarization drift, which represents the effect of impurity-particle inertia, constitutes a higher-order correction to the electric drift velocity. The influence of the former on the dynamics of impurities is determined by the dimensionless parameter  $\zeta$ , which varies with the mass-charge ratio of the impurity particles relative to that of the bulk-plasma ions. For ideal impurities  $\zeta = 0$  and the impurities are solely advected by the electric drift. For inertial impurities  $\zeta$  has a nonzero value and the polarization drift can play a role in the dynamics. The value of  $\zeta$  is in any case small, since the length scale quotient  $\rho_s/L_n$  is by assumption small. Nevertheless, the polarization drift adds important qualitative features to the dynamics of impurities. In the case of static, uniform magnetic field the electric drift is incompressible, whereas the polarization drift is compressible. Hence, the inclusion of the polarization drift in the impurity model allows for genuinely compressible effects, such as those described in Secs. IV and V.

## III. DIFFUSION OF IDEAL IMPURITIES

Theoretical studies of the diffusive effect of plasma edge turbulence on passively advected impurities have previously relied on analysis of the absolute dispersion of test particles.<sup>13,14</sup> The present approach is necessarily different, as the impurities are not modeled here as particles but as a fluid. In this section we investigate the turbulent diffusion of ideal impurities by relative-diffusion analysis of the evolution of impurity puffs.<sup>15,16</sup>

### A. Relative diffusion

We consider the release of a puff of ideal impurities into the turbulent field, which is a saturated turbulent state described by the HW model. The amount of impurities released is

$$Q \equiv \int \theta d\mathbf{x},$$

and the position  $\mathbf{c}$  of the center of mass of the impurity puff at any time instant is given by

$$\mathbf{c} \equiv \frac{1}{Q} \int \mathbf{x} \theta \, d\mathbf{x}.$$

We define the relative position vector  $\mathbf{x}' \equiv \mathbf{x} - \mathbf{c}$ , which indicates position in a reference frame moving with the center of mass of the puff. The average evolution of impurity puffs can then be characterized by the following ensemble-averaged dispersion tensors:

$$\Sigma_{ij} \equiv \frac{1}{Q} \left\langle \int x_i x_j \theta \, d\mathbf{x} \right\rangle,$$

$$S_{ij} \equiv \frac{1}{Q} \left\langle \int x'_i x'_j \theta \, d\mathbf{x} \right\rangle,$$

$$M_{ij} \equiv \langle c_i c_j \rangle.$$

Here, the components of vectors and tensors have been indicated by subindices and the angular brackets stand for the ensemble average, that is, the average over many releases. The absolute-dispersion tensor  $\Sigma_{ij}$  measures the dispersion with respect to the origin of the fixed frame, whereas the relative-dispersion tensor  $S_{ij}$  measures the dispersion relative to the center of mass. The tensor  $M_{ij}$  quantifies the “meandering” of the center of mass. The dispersion tensors are related by

$$\Sigma_{ij} = S_{ij} + M_{ij},$$

which means that absolute dispersion consists of relative dispersion and meandering of the center of mass. Relative-diffusion analysis focuses on the evolution of  $S_{ij}$ , that is, on the spreading of the puff relative to its center of mass. Specifically, it is usually the diagonal elements  $S_{ii}$  that are of interest once the reference axes are adequately selected, in our case those corresponding to the radial and poloidal directions. In view of the above relation, the meandering of the center of mass is eliminated in relative-diffusion analysis, which thus leads to better statistics in comparison with those of absolute diffusion.

The evolution of the dispersion tensors depends on the initial size and shape of the puffs, the statistical properties of the turbulent velocity field, and the collisional diffusivity  $\mu_\theta$ . Under the assumption that  $\mu_\theta$  is small, the evolution of  $S_{ii}$  for initially concentrated puffs follows three stages: first, a phase dominated by collisional diffusion that lasts while the puff is much smaller than the turbulent structures and is characterized by

$$\frac{dS_{ii}}{dt} \approx 2\mu_\theta;$$

second, a transitional phase in which the size of the puff is comparable to that of the turbulent structures and  $S_{ii}$  typically evolve faster than linearly with time (see Ref. 15 for further discussions); and last, a phase dominated by turbulent diffusion that starts when the puff is large compared to the turbulent structures and during which the

evolution of  $S_{ii}$  can be characterized by effective diffusivities  $D_i$  such that

$$\frac{dS_{ii}}{dt} = 2D_i. \quad (3)$$

These diffusivities solely depend on the statistical properties of the turbulent velocity field—more precisely, they are related to the mean squared velocities and the Lagrangian relative time scale.

The last phase, dominated by turbulent diffusion, is most relevant for us, as it eventually dominates the transport of impurities. In fact, the effective diffusivities  $D_i$  that characterize the phase of turbulent diffusion are equivalent in their definition to those employed in the experimental modeling of anomalous impurity transport.<sup>1,6</sup> Because in this last stage the diagonal elements  $S_{ii}$  grow linearly according to Eq. (3), the effective diffusivities  $D_i$  can easily be obtained from the asymptotic evolution of  $S_{ii}$ . This is the procedure used here for estimating the effective diffusivities of the turbulent field acting on ideal impurities. In principle, any initial puffs could be used for the determination of the diffusivities. From the discussion above, large initial puffs rapidly experience the final phase of turbulent diffusion, and thus provide the effective diffusivities shortly after their release. However, care must be taken in numerical simulations that the puffs do not reach the boundaries of the simulation domain, as this would result in underestimates for the diffusivities. In order to determine the effective diffusivity in one direction, we take Gaussian stripes in the perpendicular direction as initial puffs and use periodic boundary conditions. In this way, the puffs are as large as possible in one direction while the conclusions of the simulations remain valid. Moreover, because Gaussians are similarity solutions to the diffusion equation, the evolution of  $S_{ii}$  would be perfectly linear if the effect of turbulence were purely diffusive from the start.

## B. Simulation results

The HW model for plasma edge turbulence, Eqs. (1), and the model for ideal impurities, Eq. (2) with  $\zeta = 0$ , were simultaneously solved numerically using the schemes described in the Appendix. The simulations were carried out on a doubly periodic square domain of side length 40 using  $512 \times 512$  grid points. The viscosity  $\mu_\omega$  and the collisional diffusivities  $\mu_n$  and  $\mu_\theta$  were set to the common value 0.02 in all the simulations presented in this paper. We considered four different values for the adiabaticity parameter  $\mathcal{C}$  in the HW model: 0.5, 1, 2, and 4. As noted in the preceding section, low values of  $\mathcal{C}$  correspond to hydrodynamic-like regimes, whereas high values correspond to nearly adiabatic regimes. In this respect, we regard  $\mathcal{C} = 1$  as a transitional value, representative of an intermediate regime. An initial turbulent state was achieved by letting a uniform distribution of small-amplitude, random-phase modes evolve for a sufficiently

long time in order to reach a quasistationary saturated turbulent regime. Gaussian stripes having standard deviation 2 were used as initial impurity puffs. For each value of the adiabaticity parameter and each direction, radial and poloidal, 20 releases of such stripes were simulated, and the dispersion tensors were subsequently averaged.

In Fig. 1 we present snapshots of the evolution of two perpendicular stripes of impurities released into the same saturated turbulent field with  $\mathcal{C} = 1$ . The anisotropy in the diffusion of impurities is evident in the figure, as the poloidal spread of the puff in Fig. 1(e) is significantly larger than the corresponding radial spread in Fig. 1(f). Hence, diffusion acts in this case faster in the poloidal direction than in the radial direction. The degree of anisotropy is in fact controlled by the adiabaticity parameter, the turbulence ranging from isotropic in hydrodynamic limit,  $\mathcal{C} \rightarrow 0$ , to strongly anisotropic in the adiabatic limit,  $\mathcal{C} \rightarrow \infty$ .<sup>13</sup>

The evolution of the diagonal elements  $S_{ii}$  of the relative dispersion tensor for the four values of the adiabaticity parameter is shown in Fig. 2. For the three smallest values of  $\mathcal{C}$ , it is possible to distinguish the transitional and turbulent phases of growth in the plot for relative radial dispersion. In the plot corresponding to poloidal dispersion there is no clear distinction, as the evolution of  $S_{22}$  very rapidly becomes approximately linear. For the side length of our simulation domain, dispersion can start becoming underestimated when  $S_{ii}$  reach values of about 65. Nevertheless, for the three smallest values of  $\mathcal{C}$  the linear trend in  $S_{ii}$  characterizing the phase of turbulent diffusion is established before such a point is reached. In contrast, the eventually linear regime is neither apparent in the radial nor the poloidal dispersion plots for the highest value of the adiabaticity parameter,  $\mathcal{C} = 4$ . This different behavior is attributed to the weaker turbulence at higher values of  $\mathcal{C}$  and the particular transport features of the adiabatic limit, the Hasegawa–Mima equation.<sup>17</sup>

Estimates for the effective diffusivities  $D_i$  of the turbulence for the three smallest values of  $\mathcal{C}$  are obtained from linear fits to the linear portions of the curves in Fig. 2. The estimated values for the radial,  $D_1$ , and poloidal,  $D_2$ , effective diffusivities are presented in Table I. The values obtained here are qualitatively similar to those calculated in Ref. 13 by means of a test-particle, absolute-diffusion approach. In particular, the decrease of  $D_1$  with  $\mathcal{C}$  as well as the rise of  $D_2$  with  $\mathcal{C}$  for  $\mathcal{C} \geq 1$  are here reproduced. We note that the accuracy of the present approach could be improved by simulating the evolution of the impurity puffs for longer times on a larger domain. The number of puff releases could as well be increased in order to ensure convergence to the ensemble averages. We also note that different values for  $\mu_\omega$  and  $\mu_n$  were used in the latter reference, with collisional diffusion of impurities being discarded because of their test-particle modeling.

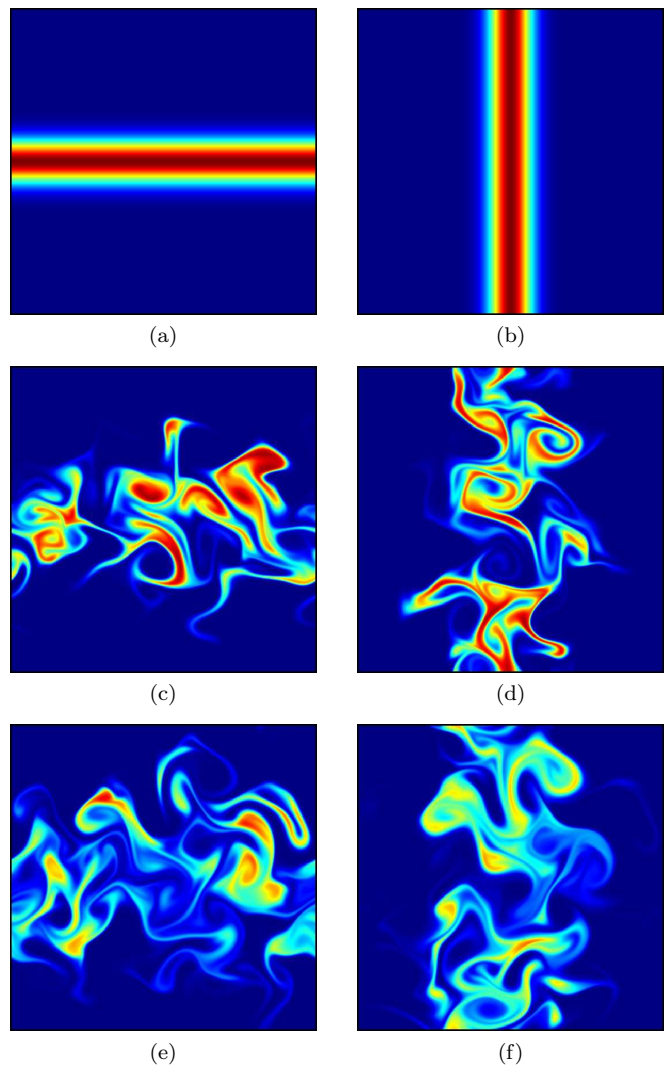


FIG. 1: (Color online) Evolution of Gaussian stripes of ideal impurities in a HW saturated turbulent state with  $\mathcal{C} = 1$ : radial stripe at (a)  $t = 0$ , (c)  $t = 6$ , and (e)  $t = 12$ ; and poloidal stripe at (b)  $t = 0$ , (d)  $t = 6$ , and (f)  $t = 12$ .

TABLE I: Effective diffusivities in the radial direction  $D_1$  and the poloidal direction  $D_2$  of HW saturated turbulence for different values of  $\mathcal{C}$ .

$\mathcal{C}$	$D_1$	$D_2$
0.5	1.12	2.32
1	0.65	2.26
2	0.36	2.63

#### IV. CLUSTERING OF INERTIAL IMPURITIES

The importance of inertia in the advection of particles by turbulent flows is well known in fluid dynamics.<sup>18</sup> As in magnetized plasmas, the transport of inertial particles by fluids shows compressible features even when the advecting flow is incompressible. Particle inertia has been

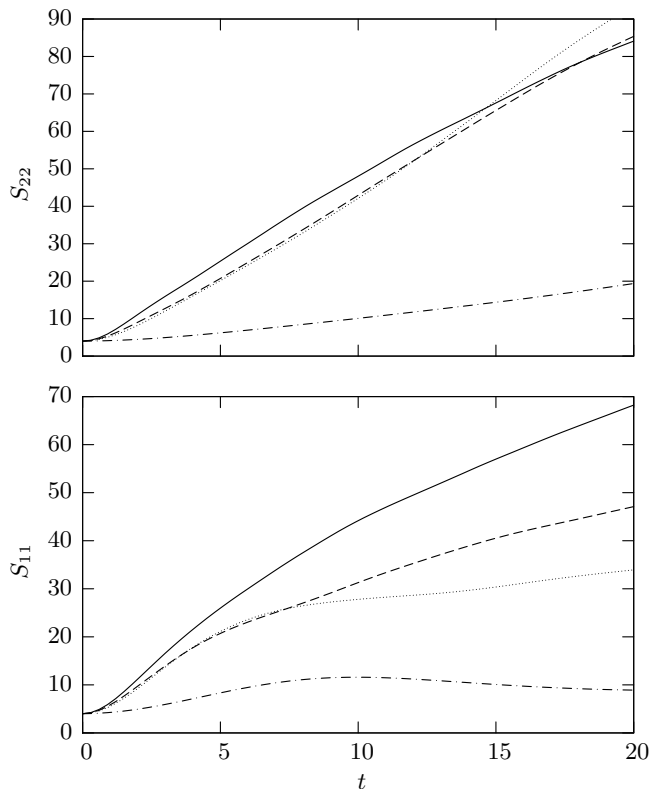


FIG. 2: Evolution of the relative radial dispersion  $S_{11}$  and the relative poloidal dispersion  $S_{22}$  of ideal impurity Gaussian stripes released in HW saturated turbulence with  $C = 0.5$  (solid),  $C = 1$  (dashed),  $C = 2$  (dotted), and  $C = 4$  (dash-dotted).

shown to result in clustering in vortical structures, and its role in phenomena such as planetary formation has been suggested.<sup>19</sup> While the dynamics of impurity particles in magnetized plasmas are not governed by the same forces as in fluids, inertia enters the dynamics of impurities in magnetized plasmas in a similar way as the Coriolis force enters those of heavy impurities in rotating fluids. Hence, corresponding clustering effects for inertial impurities in magnetized plasmas should be expected. In this section we discover and explain the correlation between impurity density and vorticity that results from the compressibility introduced by the polarization drift in the case of inertial impurities. In order to most clearly reveal this effect we consider a homogeneous initial distribution of impurities, since such a distribution would remain unchanged in the incompressible, that is, ideal-impurity case.

### A. Simulation results

Simulations of the HW model for plasma edge turbulence, Eqs. (1), and the impurity model, Eq. (2), were again performed on a doubly periodic square domain of side length 40 using  $512 \times 512$  grid points. The adiabaticity parameter  $C$  in the HW model was set to the

transitional value 1, while we contemplated various values for the parameter  $\zeta$ , ranging from  $-0.01$  to  $0.05$ . The impurity density field  $\theta$  was initialized with the constant value  $\theta_0 = 1$ , and the initial turbulent fields were taken from a HW saturated turbulent state.

In Fig. 3 we present side by side snapshots of the evolution of the vorticity  $\omega$  of the electric drift velocity and the impurity density field for the case  $\zeta = 0.01$ . Merely 5 time units after the simulation is started, there is already indication of a correlation between vorticity and impurity density. At  $t = 50$ , there is visually little difference between the two fields. Figure 4 shows a scatter plot of vorticity and relative impurity density  $\theta/\theta_0$  at  $t = 100$  for three different values of  $\zeta$ . The plot clearly suggests an approximate linear relation given by

$$\theta/\theta_0 \approx 1 + K\omega,$$

with the regression coefficient  $K$  depending on  $\zeta$ . The least-squares estimates of the coefficient  $K$  are plotted as a function of the parameter  $\zeta$  in Fig. 5. This figure in turn indicates a linear relation between  $K$  and  $\zeta$  in the form  $K \approx 0.82\zeta$ . In summary, we find that the density of inertial impurities eventually becomes linearly correlated with the vorticity, the regression coefficient being proportional to the parameter  $\zeta$ .

### B. Turbulent mixing and clustering

The behavior just described can easily be explained using an argument of turbulent mixing, or turbulent equipartition.<sup>20,21,22</sup> Performing basic algebraic manipulations on Eq. (2) while accounting for the particular definition of the Lagrangian derivative  $D_t$  in Eq. (1d), we may rewrite the impurity model equation in the form

$$D_t(\ln \theta - \zeta\omega) = \zeta \nabla_{\perp} \ln \theta \cdot D_t \nabla_{\perp} \varphi + \frac{\mu\theta}{\theta} \nabla_{\perp}^2 \theta, \quad (4)$$

where the left-hand side describes advection by the electric drift and compression by the polarization drift, while the right hand-side describes advection by the polarization drift as well as collisional diffusion. We will now argue that the right-hand side of this equation is small, which implies that  $\ln \theta - \zeta\omega$  is approximately a Lagrangian invariant, or in other words, that  $\ln \theta - \zeta\omega$  is nearly conserved along the trajectories defined by the electric drift velocity. We split the impurity density  $\theta$  into its mean value  $\theta_0$  and the fluctuations  $\theta_1$  arising from compressibility. Based on the computational results, we further postulate that  $\theta_1/\theta_0 = \mathcal{O}(\zeta)$ . Selectively applying the split  $\theta \equiv \theta_0 + \theta_1$  to Eq. (4), we obtain

$$D_t(\ln \theta - \zeta\omega) = \zeta \nabla_{\perp} \ln \left( 1 + \frac{\theta_1}{\theta_0} \right) \cdot D_t \nabla_{\perp} \varphi + \frac{\mu\theta}{\theta} \nabla_{\perp}^2 \theta_1.$$

Assuming that the normalizations used in the impurity model adequately represent the scales of fluctuations, the



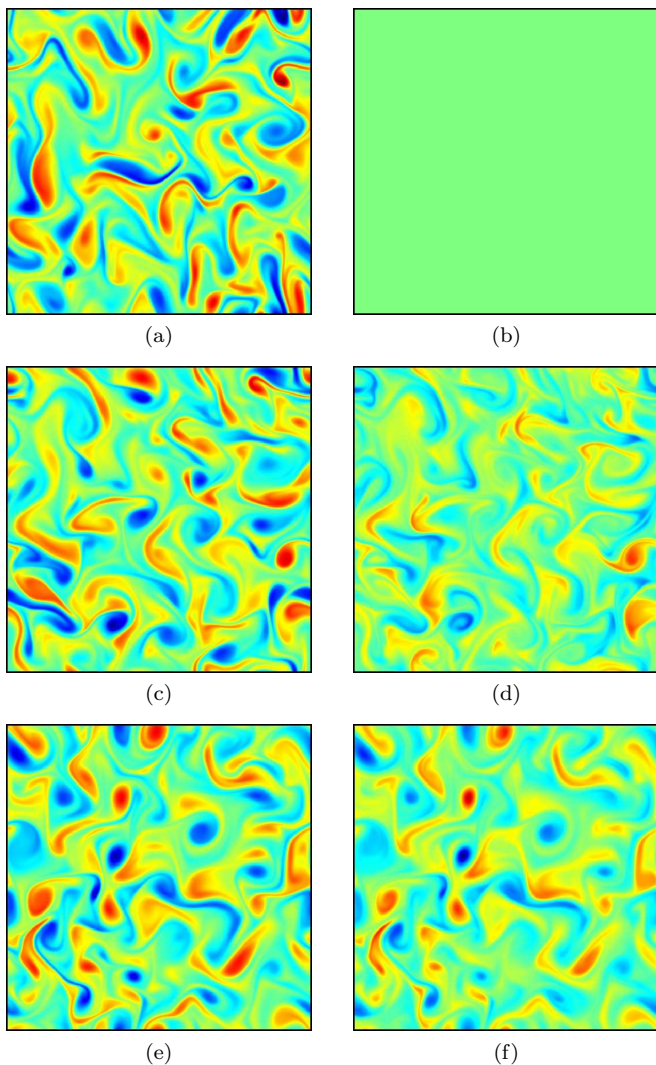


FIG. 3: (Color online) Evolution of the vorticity  $\omega$  and the density  $\theta$  of inertial impurities ( $\zeta = 0.01$ ) in a HW saturated turbulent state with  $C = 1$ : (a)  $\omega$  and (b)  $\theta$  at  $t = 0$ , (c)  $\omega$  and (d)  $\theta$  at  $t = 5$ , and (e)  $\omega$  and (f)  $\theta$  at  $t = 50$ . Green corresponds to mean values, while red and blue represent positive and negative fluctuations respectively.

right-hand side of this last equation is of order  $\zeta^2 + \zeta\mu\theta$ , whereas the fluctuating component of the quantity inside the Lagrangian derivative on left-hand side is of order  $\zeta$ . Hence,  $\ln\theta - \zeta\omega$  varies slowly along the electric drift trajectories, thus constituting an approximate Lagrangian invariant.

Turbulent mixing homogenizes Lagrangian invariants, and thus tends to drive systems to states of so-called turbulent equipartition. The application of this argument to the approximate invariant here yields

$$\ln\theta - \zeta\omega \approx \text{const.}$$

Because the amount of impurities is conserved and it is assumed that  $\theta_1/\theta_0 = \mathcal{O}(\zeta)$ , the previous expression can

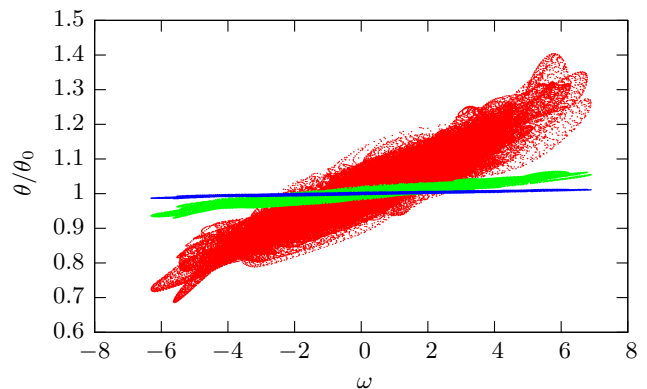


FIG. 4: (Color online) Scatter plot of vorticity  $\omega$  and relative density  $\theta/\theta_0$  of inertial impurities in a HW saturated turbulent state with  $C = 1$  for  $\zeta = 0.05$  (red/steepest),  $\zeta = 0.01$  (green), and  $\zeta = 0.002$  (blue/flattest).

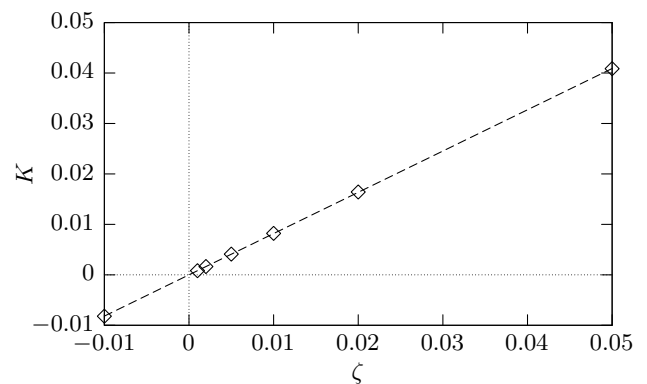


FIG. 5: Least-squares estimates of the coefficient  $K$  as a function of  $\zeta$  for the impurity-density-vorticity linear regression  $\theta/\theta_0 \approx 1 + K\omega$  in a HW saturated turbulent state with  $C = 1$ . The fitted line (dashed) corresponds to  $K = 0.82\zeta$ .

be recast into the simpler form

$$\theta/\theta_0 \approx 1 + \zeta\omega.$$

The present analysis thus predicts a linear relation between the impurity density and the vorticity, the regression coefficient being the parameter  $\zeta$ . Hence, the theoretical argument explains the effect discovered in the simulations up to a slight mismatch in the regression coefficient. We emphasize that the particular features of the HW turbulence model were not used in the previous argument, the conclusions relying solely on the modeling of the dynamics of impurities and the argument of turbulent mixing. It follows that the clustering of inertial impurities in vortical structures is a generic effect, independent of the underlying instability mechanisms and the specific characteristics of the turbulence.

The fact that the density of inertial impurities becomes directly correlated with the vorticity implies that impurities of positive charge cluster in positive vortices, the opposite taking place for negatively charged impurities. As previously introduced, this effect is similar to the ag-

gregation of heavy particles in anticyclonic vortices that can take place in rotating fluids as a result of the Coriolis force.<sup>18</sup> In contrast with compression by the polarization drift, which yields  $D_t \ln \theta \sim \zeta D_t \omega$ , compression by the Coriolis force enters the dynamics of heavy impurities in the form  $D_t \ln \theta \sim -2\Omega\omega$ , with  $\Omega$  being the overall rotation. Hence, aggregation in the rotating-fluid case does not necessarily lead to a linear relation between impurity density and vorticity, but can go on further to form highly concentrated clusters in the cores of anticyclonic vortices. For this reason, it has for example been suggested as a mechanism, in combination with gravitation, for planetary formation in rotating astrophysical disks.<sup>19</sup>

## V. PINCH OF INERTIAL IMPURITIES

In this section we finally investigate the possible role of inertia in the radially inward pinch that concentrates impurities in the center of the plasma column in magnetic confinement devices.<sup>1,5</sup> As a measure of the overall drift of impurities, we consider the global impurity flux

$$\mathbf{\Gamma}_\theta \equiv \mathbf{\Gamma}_\theta^E + \mathbf{\Gamma}_\theta^p \equiv \int \theta \mathbf{v}_E d\mathbf{x} + \int \theta \mathbf{v}_p d\mathbf{x}.$$

Here, we have distinguished the components respectively resulting from advection by the electric drift and by the polarization drift. In terms of these global fluxes, we define the impurity drift velocity  $\mathbf{V}_\theta$  and its components  $\mathbf{V}_\theta^E$  and  $\mathbf{V}_\theta^p$  by means of

$$\mathbf{V}_\theta \equiv \mathbf{V}_\theta^E + \mathbf{V}_\theta^p \equiv Q^{-1} \mathbf{\Gamma}_\theta^E + Q^{-1} \mathbf{\Gamma}_\theta^p,$$

where once again  $Q \equiv \int \theta d\mathbf{x}$ . For a homogeneous distribution of impurities in a periodic domain, both  $\mathbf{\Gamma}_\theta^E$  and  $\mathbf{\Gamma}_\theta^p$  are zero. Hence, ideal impurities cannot experience a net drift when their initial distribution is homogeneous, since such a distribution remains unchanged in the ideal case. In contrast, inertial impurities may experience a drift even if their initial distribution is uniform, given that the latter is altered by compressible effects, as shown in the preceding section.

### A. Simulation results

We begin by monitoring the radial drift velocity  $\mathbf{V}_\theta \cdot \hat{\mathbf{x}}$  in the simulations referred to in Sec. IV. These were initialized with homogeneous distributions of inertial impurities in a HW saturated turbulent state with  $\mathcal{C} = 1$ . In Fig. 6 we present the evolution of the radial drift velocity for four different values of  $\zeta$ . In every case, the evolution of the radial drift comprises a strong transient burst, after which the drift enters a saturated quasistationary regime. Moreover, the radial drift velocity is seen to have a definite sign opposite to that of  $\zeta$ , that is to say, opposite to the type of charge of the impurity particles. It follows that positively charged impurities are subject to

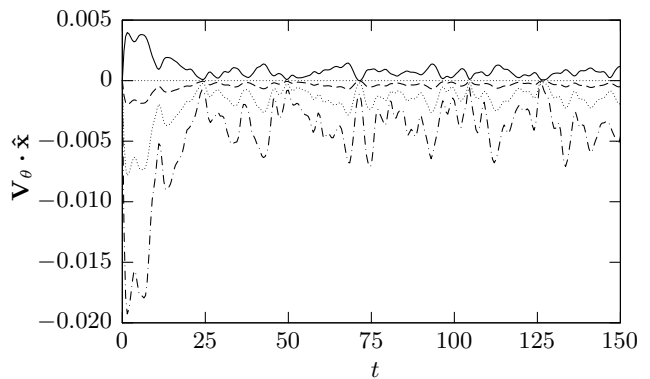


FIG. 6: Evolution of the radial drift velocity  $\mathbf{V}_\theta \cdot \hat{\mathbf{x}}$  of inertial impurities in a HW saturated turbulent state with  $\mathcal{C} = 1$  for  $\zeta = -0.01$  (solid),  $\zeta = 0.005$  (dashed),  $\zeta = 0.02$  (dotted), and  $\zeta = 0.05$  (dash-dotted).

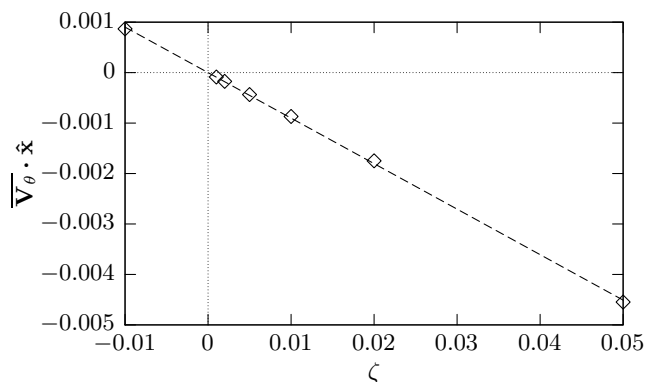


FIG. 7: Time-averaged radial drift velocity  $\overline{\mathbf{V}_\theta \cdot \hat{\mathbf{x}}}$  of inertial impurities as a function of  $\zeta$  in a HW saturated turbulent state with  $\mathcal{C} = 1$ . The fitted line (dashed) corresponds to  $\overline{\mathbf{V}_\theta \cdot \hat{\mathbf{x}}} = -0.090\zeta$ .

a continuous radially inward drift, as observed in experimental investigations of impurity transport.<sup>1,5</sup> In Fig. 7 we show the time-averaged radial drift velocities  $\overline{\mathbf{V}_\theta \cdot \hat{\mathbf{x}}}$  in the saturated regimes, computed using the values of the drifts between  $t = 25$  and  $t = 150$ . The variation of the time-averaged radial drift with  $\zeta$  is remarkably linear, well fitted by  $\overline{\mathbf{V}_\theta \cdot \hat{\mathbf{x}}} = -0.090\zeta$ . Therefore, the present radial drift scales linearly with the mass-charge ratio of the impurity particles.

The reason for this peculiar pinch effect is not clear at the outset. An analysis of the components  $\mathbf{V}_\theta^E$  and  $\mathbf{V}_\theta^p$  of the drift velocity in the simulations reveals that the contribution of the electric drift is by far dominant. Hence, while the net drift arises as a result of the polarization drift, the main role of the latter is not to globally advect impurities, but rather to distribute them in such a way that they experience net transport by the electric drift. From a naive point of view, it could be thought that the correlation between impurity density and vorticity discovered in Sec. IV is responsible for the radial drift. Indeed, transport of trapped particles by coher-



ent vortices is for instance known to play an important role in transport processes in rotating fluids.<sup>18</sup> However, because an incompressible flow in a 2D periodic domain cannot globally transport its vorticity, a purely linear relation between impurity density and vorticity would yield no drift at all. Thus, the explanation for the radial drift of inertial impurities requires deeper thought.

### B. Net transport and pinch

Intrigued by the initial burst and the subsequent saturation of the radial impurity drift velocity, we analyze the evolution of the global impurity flux. In particular, we focus on the  $\mathbf{\Gamma}_\theta^E$  component, given that the net transport of impurities is dominated by the electric drift. In a periodic domain, the evolution of  $\mathbf{\Gamma}_\theta^E$  under the impurity model in Eq. (2) is governed by

$$\frac{d\mathbf{\Gamma}_\theta^E}{dt} = \mathbf{\Lambda}_1 + \mathbf{\Lambda}_2 + \mathbf{\Lambda}_3 + \mathbf{\Lambda}_4,$$

where

$$\begin{aligned} \mathbf{\Lambda}_1 &\equiv \int \theta \mathbf{D}_t \mathbf{v}_E \, d\mathbf{x}, \\ \mathbf{\Lambda}_2 &\equiv \int \zeta \theta \mathbf{v}_E \mathbf{D}_t \omega \, d\mathbf{x}, \\ \mathbf{\Lambda}_3 &\equiv \int \zeta (\nabla_\perp \theta \cdot \mathbf{D}_t \nabla_\perp \varphi) \mathbf{v}_E \, d\mathbf{x}, \\ \mathbf{\Lambda}_4 &\equiv \int \mu_\theta \mathbf{v}_E \nabla_\perp^2 \theta \, d\mathbf{x}. \end{aligned}$$

These four contributions correspond respectively to evolution of the electric drift velocity, compression by the polarization drift, advection by the polarization drift, and collisional diffusion of impurities. In order to reveal the magnitude of the different terms, we again split the impurity density into its mean value  $\theta_0$  and the fluctuations  $\theta_1$ , keeping in mind that  $\theta_1/\theta_0 = \mathcal{O}(\zeta)$ . Selectively applying the split  $\theta \equiv \theta_0 + \theta_1$  to the above definitions we obtain

$$\begin{aligned} \mathbf{\Lambda}_1 &= \int \theta_1 \mathbf{D}_t \mathbf{v}_E \, d\mathbf{x} = \mathcal{O}(\zeta), \\ \mathbf{\Lambda}_2 &= \int \zeta \theta \mathbf{v}_E \mathbf{D}_t \omega \, d\mathbf{x} = \mathcal{O}(\zeta), \\ \mathbf{\Lambda}_3 &= \int \zeta (\nabla_\perp \theta_1 \cdot \mathbf{D}_t \nabla_\perp \varphi) \mathbf{v}_E \, d\mathbf{x} = \mathcal{O}(\zeta^2), \\ \mathbf{\Lambda}_4 &= \int \mu_\theta \mathbf{v}_E \nabla_\perp^2 \theta_1 \, d\mathbf{x} = \mathcal{O}(\zeta \mu_\theta). \end{aligned}$$

According to these estimates,  $\mathbf{\Lambda}_1$  and  $\mathbf{\Lambda}_2$  dominate the dynamics of the global impurity flux. In the case of uniform impurity density,  $\mathbf{\Lambda}_2$  is the only nonvanishing contribution to  $d\mathbf{\Gamma}_\theta^E/dt$ , being therefore responsible for the initial development of drift velocities.

We will now resort to the particular HW turbulence model to show that  $\mathbf{\Lambda}_2$  constitutes a source for global radial flux in the present case. Substitution of the HW vorticity equation in the above expression for  $\mathbf{\Lambda}_2$  yields

$$\begin{aligned} \mathbf{\Lambda}_2 &= \int \zeta \theta [\mathcal{C}(\varphi - n) + \mu_\omega \nabla_\perp^2 \omega] \mathbf{v}_E \, d\mathbf{x} \\ &= -\zeta \mathcal{C} \theta_0 \int n \mathbf{v}_E \, d\mathbf{x} + \mathcal{O}(\zeta^2 + \zeta \mu_\omega). \end{aligned}$$

Projecting this equation onto the radial direction we find

$$\begin{aligned} \mathbf{\Lambda}_2 \cdot \hat{\mathbf{x}} &= -\zeta \mathcal{C} \theta_0 \int n \partial_y \varphi \, d\mathbf{x} + \mathcal{O}(\zeta^2 + \zeta \mu_\omega) \\ &= -\zeta \mathcal{C} \theta_0 \Gamma_n + \mathcal{O}(\zeta^2 + \zeta \mu_\omega). \end{aligned}$$

Here, we have identified the sole source  $\Gamma_n$  of energy and generalized enstrophy within the HW model. Since  $\Gamma_n$  is in practice positive definite (see, e.g., Table I in Ref. 11), it follows that  $\mathbf{\Lambda}_2 \cdot \hat{\mathbf{x}}$  has a definite sign opposite to that of  $\zeta$ , thus acting as a source for the global radial flux of inertial impurities. As explained before,  $\mathbf{\Lambda}_2$  is initially the only nonzero contribution to  $d\mathbf{\Gamma}_\theta^E/dt$ , thus explaining the transient bursts observed in Fig. 6. More generally, this term sustains the radial transport of impurities in the turbulent states described by the HW model.

From the above estimates, we are led to expect that  $\mathbf{\Lambda}_1$  is responsible for the saturation of the radial impurity drift seen in Fig. 6. The reason for this saturation becomes clear when we account for the correlation that develops between impurity density and vorticity. The argument of turbulent equipartition used in Sec. IV predicted an eventual relation  $\theta_1/\theta_0 \approx \zeta \omega$  between the impurity density fluctuations and the vorticity. Considering this relation and the fact that vorticity is not globally transported by the electric drift we obtain

$$\begin{aligned} \mathbf{\Lambda}_1 &\approx \int \zeta \theta_0 \omega \mathbf{D}_t \mathbf{v}_E \, d\mathbf{x} \\ &= \zeta \theta_0 \frac{d}{dt} \int \omega \mathbf{v}_E \, d\mathbf{x} - \zeta \theta_0 \int \mathbf{v}_E \mathbf{D}_t \omega \, d\mathbf{x} \\ &= - \int \zeta \theta_0 \mathbf{v}_E \mathbf{D}_t \omega \, d\mathbf{x} \approx -\mathbf{\Lambda}_2 \end{aligned}$$

whenever turbulent equipartition holds true. Consequently, when such a state is reached, the two terms dominating the evolution of the radial drift approximately cancel, and the radial drift enters a quasistationary regime. The time it takes for this regime to be reached is independent of  $\zeta$ , as the development of correlation is exclusively dependent on the turbulent mixing by the electric drift. In fact, the evolution of  $\theta_1$  is approximately linear with  $\zeta$  within short time intervals, since in line with the discussion in Sec. IV it follows that

$$\mathbf{D}_t \theta_1 = \zeta \theta_0 \mathbf{D}_t \omega + \mathcal{O}(\zeta^2 + \zeta \mu_\theta).$$

Given that solely the density fluctuations yield net transport of impurities, the evolution of the impurity drift is

likewise approximately linear with  $\zeta$ . This explains the apparent linear scaling of the curves in Fig. 6 and the linearity of the time-averaged radial drift in Fig. 7.

While the arguments presented here do not yield a prediction for the quasistationary level of the radial impurity drift, they do identify the mechanism for its onset and likewise explain its scaling with the parameter  $\zeta$ . We emphasize that the former mechanism relies on the specific properties of the turbulence described by the HW model. Nevertheless, an analogue pinch effect would appear for other driving instabilities provided that the term  $\Lambda_2$  remains a source for a definite impurity drift.

## VI. CONCLUSION

We have studied the transport of impurity particles in plasma edge turbulence, basing our investigations on the paradigmatic Hasegawa–Wakatani (HW) model for resistive drift-wave turbulence and a consistent passive-fluid model for the impurities. The latter model takes into account impurity-particle inertia, which enters the impurity flow velocity in the form of the polarization drift. Inertia has indeed been found to play a significant role in the turbulent transport of impurities, since it gives rise to subtle yet qualitatively important compressible effects.

The model equations have been investigated both theoretically and computationally. The numerical simulations were performed using the semi-Lagrangian (SL) pseudospectral code briefly described in the Appendix. Although the emphasis of this paper is not on the numerical methods employed, we point out the suitability of SL schemes for the advection-dominated problems that appear in plasma turbulence. In particular, we highlight the superior stability of the SL semi-implicit scheme used here for the HW model, which is known to constitute a numerically challenging nonlinear problem.

In the case of ideal impurities, we have focused on their turbulent diffusion by the electric drift. This effect has been demonstrated by relative-diffusion analysis of the evolution of impurity puffs. The effective diffusivities of the turbulent advecting field have been calculated for several values of the adiabaticity parameter in the HW model. The resulting turbulent diffusivities are in qualitative agreement with those obtained in an earlier study based on an absolute-diffusion, test-particle approach.<sup>13</sup>

In the case of inertial impurities, we have discovered that their density eventually correlates with the vorticity of the electric drift velocity. This clustering effect scales linearly with the mass–charge ratio of the impurity particles and results from compression by the polarization drift in combination with turbulent mixing. The clustering of impurities in vortices of definite sign is a generic effect in magnetized-plasma turbulence, in the sense that it is independent of the specific characteristics of the turbulence.

Finally, we have also found an overall radial drift of inertial impurities that scales linearly with the mass–

charge ratio of the impurity particles and is inward for positively charged impurities. This anomalous pinch relies on the particular features of the turbulence described by the HW model. In contrast with other known turbulent pinches,<sup>6</sup> the present pinch is neither caused by a specific magnetic field geometry nor by temperature gradients, given that our models assume a uniform magnetic field and cold impurities. Consequently, our finding of a net radial drift due to impurity-particle inertia constitutes a new contribution towards the understanding of the anomalous pinch of impurities in magnetic confinement devices.

## Acknowledgments

The first author is grateful to M. P. Sørensen for co-supervising his M.Sc. thesis, which constitutes the basis for this publication. O.E.G. was sponsored by the Research Council of Norway.

## APPENDIX: NUMERICAL SCHEMES

The numerical simulations presented in this paper were performed using a semi-Lagrangian (SL) pseudo-spectral code developed by the first author.<sup>23</sup> In essence, SL schemes combine the very stable Lagrangian treatment of advection with the convenience of a fixed spatial discretization.<sup>24,25</sup> This is achieved by integrating the partial differential equations in question along a different family of advective trajectories in each time step, precisely those that by the end of the time step traverse the fixed points on which the spatial discretization is based. We now outline how the aforementioned code combines SL method and the pseudospectral discretization to numerically solve the HW model and the impurity passive-fluid model described in Sec. II.

We discretize time using a constant time step  $\Delta t$ , which yields the sequence  $\{t_m\}$  of time instants related by  $t_{m+1} = t_m + \Delta t$ . Likewise, we use the Fourier pseudo-spectral method to discretize the doubly periodic rectangular simulation domain.<sup>24</sup> This results in a regular grid  $\{\mathbf{x}_i\}$  of collocation points. In our application of the SL method we consider the (incompressible) electric drift velocity  $\mathbf{v}_E = \hat{\mathbf{z}} \times \nabla_{\perp} \varphi$  as the sole advecting field. Hence, the advective trajectory  $\mathbf{X}(\mathbf{x}_i, t_{m+1}; t)$  that passes through the grid point  $\mathbf{x}_i$  at time  $t_{m+1}$  is given by

$$\begin{aligned} \frac{d}{dt} \mathbf{X}(\mathbf{x}_i, t_{m+1}; t) &= \mathbf{v}_E(\mathbf{X}(\mathbf{x}_i, t_{m+1}; t), t), \\ \mathbf{X}(\mathbf{x}_i, t_{m+1}; t_{m+1}) &= \mathbf{x}_i. \end{aligned}$$

At each time step, we firstly determine the so-called upstream points  $\{\mathbf{X}(\mathbf{x}_i, t_{m+1}; t_m) \equiv \mathbf{x}_i - \boldsymbol{\alpha}_i\}$ . These are numerically calculated using the following second-order scheme, which combines the implicit midpoint rule and

linear extrapolation of the advecting field.<sup>26,27</sup>

$$\begin{aligned}\boldsymbol{\alpha}_i &= \Delta t \mathbf{v}_E^*(\mathbf{x}_i - \frac{1}{2}\boldsymbol{\alpha}_i, t_{m+1/2}), \\ \mathbf{v}_E^*(\mathbf{x}, t_{m+1/2}) &= \frac{3}{2}\mathbf{v}_E(\mathbf{x}, t_m) - \frac{1}{2}\mathbf{v}_E(\mathbf{x}, t_{m-1}),\end{aligned}$$

where  $t_{m+1/2} = t_m + \frac{1}{2}\Delta t$ . The implicit equations for the displacements  $\{\boldsymbol{\alpha}_i\}$  are solved using Newton's method, which converges in very few iterations.

Subsequently, the model equations are integrated from  $t_m$  to  $t_{m+1}$  along the advective trajectories. For the HW model, Eq. (1), we use the following unconditionally stable second-order semi-implicit scheme:

$$\begin{aligned}n^{m+1} - \tilde{n}^m &= \frac{1}{2}\Delta t \mathcal{C} \left[ (\varphi - n)^{m+1} + \widetilde{(\varphi - n)^m} \right] \\ &\quad + \frac{1}{2}\Delta t \mu_n \left[ \nabla_{\perp}^2 n^{m+1} + \widetilde{\nabla_{\perp}^2 n^m} \right] \\ &\quad + x^{m+1} - \tilde{x}^m, \\ \omega^{m+1} - \tilde{\omega}^m &= \frac{1}{2}\Delta t \mathcal{C} \left[ (\varphi - n)^{m+1} + \widetilde{(\varphi - n)^m} \right] \\ &\quad + \frac{1}{2}\Delta t \mu_{\omega} \left[ \nabla_{\perp}^2 \omega^{m+1} + \widetilde{\nabla_{\perp}^2 \omega^m} \right].\end{aligned}$$

Here the superscripts indicate time, and tildes denote evaluation at the upstream points. Hence, for a function  $\mathbf{g}(\mathbf{x}, t)$  we have  $\tilde{\mathbf{g}}^m(\mathbf{x}_i) = \mathbf{g}(\mathbf{x}_i - \boldsymbol{\alpha}_i, t_m)$ . The above equations supplemented with  $\omega^{m+1} = \nabla_{\perp}^2 \varphi^{m+1}$  are easily solved within the Fourier discretization.

For the impurity passive-fluid model, Eq. (2), we employ the following second-order implicit-explicit scheme:

$$\begin{aligned}\theta^* - \tilde{\theta}^m &= -\Delta t \nabla_{\perp} \cdot \widetilde{(\theta \mathbf{v}_p)^m} + \frac{1}{2}\Delta t \mu_{\theta} \left[ \nabla_{\perp}^2 \theta^* + \widetilde{\nabla_{\perp}^2 \theta^m} \right], \\ \theta^{m+1} - \tilde{\theta}^m &= -\frac{1}{2}\Delta t \left[ \nabla_{\perp} \cdot (\theta^* \mathbf{v}_p)^{m+1} + \nabla_{\perp} \cdot \widetilde{(\theta \mathbf{v}_p)^m} \right] \\ &\quad + \frac{1}{2}\Delta t \mu_{\theta} \left[ \nabla_{\perp}^2 \theta^{m+1} + \widetilde{\nabla_{\perp}^2 \theta^m} \right].\end{aligned}$$

In our code we further approximate the polarization drift  $\mathbf{v}_p = -\zeta \mathbf{D}_t \nabla_{\perp} \varphi$  by means of

$$\mathbf{v}_p^{m+1} = \zeta (\widetilde{\nabla_{\perp} \varphi^m} - \nabla_{\perp} \varphi^{m+1}) / \Delta t + \mathcal{O}(\Delta t).$$

While in theory this approximation reduces the accuracy of the scheme to first order, its effect in practice is very limited given the smallness of the polarization drift.

We lastly note that the combination of spectral discretizations with SL schemes is problematic.<sup>24</sup> The difficulty lies in the required evaluations at midpoints and upstream points, which are generally not equispaced. Performing such evaluations exactly, using the spectral representation, is in most cases computationally infeasible. In our code this problem is circumvented using high-order periodic spline interpolation on a refined grid.<sup>28,29</sup>

- 
- <sup>1</sup> F. Wagner and U. Stroth, *Plasma Phys. Control. Fusion* **35**, 1321 (1993).  
<sup>2</sup> W. Horton, *Rev. Mod. Phys.* **71**, 735 (1999).  
<sup>3</sup> ITER Physics Expert Group on Divertor, ITER Physics Expert Group on Divertor Modelling and Database, and ITER Physics Basis Editors, *Nucl. Fusion* **39**, 2391 (1999).  
<sup>4</sup> K.-D. Zastrow, *Nucl. Fusion* **39**, 1891 (1999).  
<sup>5</sup> R. Dux, *Fusion Sci. Technol.* **44**, 708 (2003).  
<sup>6</sup> X. Garbet, P. Mantica, C. Angioni, *et al.*, *Plasma Phys. Control. Fusion* **46**, B557 (2004).  
<sup>7</sup> G. I. Taylor, *Proc. London Math. Soc.* **20**, 196 (1921).  
<sup>8</sup> L. F. Richardson, *Proc. R. Soc. London, Ser. A* **110**, 709 (1926).  
<sup>9</sup> A. Hasegawa and M. Wakatani, *Phys. Rev. Lett.* **50**, 682 (1983).  
<sup>10</sup> A. Hasegawa and K. Mima, *Phys. Fluids* **21**, 87 (1978).  
<sup>11</sup> S. J. Camargo, D. Biskamp, and B. D. Scott, *Phys. Plasmas* **2**, 48 (1995).  
<sup>12</sup> O. E. Garcia, *J. Plasma Phys.* **65**, 81 (2001).  
<sup>13</sup> R. Basu, V. Naulin, and J. J. Rasmussen, *Commun. Non-linear Sci. Numer. Simul.* **8**, 477 (2003).  
<sup>14</sup> R. Basu, T. Jessen, V. Naulin, and J. Juul Rasmussen, *Phys. Plasmas* **10**, 2696 (2003).  
<sup>15</sup> G. T. Csanady, *Turbulent Diffusion in the Environment*, (D. Reidel Pub. Co., Dordrecht, Holland, 1973).  
<sup>16</sup> T. Mikkelsen, S. E. Larsen, and H. L. Pecseli, *Q. J. R. Meteor. Soc.* **113**, 81 (1987).  
<sup>17</sup> S. V. Annibaldi, G. Manfredi, R. O. Dendy, and L. O. Drury, *Plasma Phys. Control. Fusion* **42**, L13 (2000).  
<sup>18</sup> A. Provenzale, *Ann. Rev. Fluid Mech.* **31**, 55 (1999).  
<sup>19</sup> A. Bracco, P. H. Chavanis, A. Provenzale, and E. A. Spiegel, *Phys. Fluids* **11**, 2280 (1999).  
<sup>20</sup> V. V. Yankov, *JETP Lett.* **60**, 171 (1994).  
<sup>21</sup> M. B. Isichenko and N. V. Petviashvili, *Phys. Plasmas* **2**, 3650 (1995).  
<sup>22</sup> M. B. Isichenko and V. V. Yankov, *Phys. Rep.* **283**, 161 (1997).  
<sup>23</sup> M. Priego, M.Sc. thesis, Technical University of Denmark, Kgs. Lyngby, 2004.  
<sup>24</sup> J. P. Boyd, *Chebyshev and Fourier Spectral Methods* (Dover, New York, 2001), 2nd ed.  
<sup>25</sup> A. Staniforth and J. Cote, *Mon. Weather Rev.* **119**, 2206 (1991).  
<sup>26</sup> C. Temperton and A. Staniforth, *Q. J. R. Meteor. Soc.* **113**, 1025 (1987).  
<sup>27</sup> A. McDonald and J. R. Bates, *Mon. Weather Rev.* **115**, 737 (1987).  
<sup>28</sup> G. Beylkin, *Appl. Comput. Harmon. Anal.* **2**, 363 (1995).  
<sup>29</sup> G. Steidl, *Adv. Comput. Math.* **9**, 337 (1998).